Design optimisation of additively manufactured titanium lattice structures for biomedical implants

El-Sayed, M.A., Essa, K., Ghazy, M. and Hassanin, H.

Design Optimisation of Additively Manufactured Titanium Lattice Structures for Biomedical Implants

Mahmoud Ahmed El-Sayed[1], Khamis Essa[2], Mootaz Ghazy[1], and Hany Hassanin[3]

1 Department of Industrial and Management Engineering, Arab Academy for Science and Technology and Maritime Transport, PO box 1029, Abu Qir, Alexandria 21599, Egypt.

2 University of Birmingham, Birmingham, B15 2TT, UK.

3 school of engineering technology and design, Canterbury Christ Church University, Canterbury, CT1 1QU, UK.

Corresponding author: Hany Hassanin enghanisalama@yahoo.com

Abstract

A key advantage of additive manufacturing (AM) is that it allows the fabrication of lattice structures for customised biomedical implants with high performance. This paper presents the use of statistical approaches in design optimisation of additively manufactured titanium lattice structures for biomedical implants. Design of experiments using response surface and analysis of variance were carried out to study the effect design parameters on the properties of the AM lattice structures such as ultimate compression strength, specific compressive strength, elastic modulus, and porosity. In addition, the lattice dimensions were optimized to fabricate a diamond cellular structure with properties that match human bones. The study found that the length of a diamond-shaped unit cell strut is the most significant design parameter. In particular, the porosity of the unit cell increases as the strut length increases, while it had a significant reverse effect on the specific compressive strength, elastic modulus and ultimate compression strength. On the other hands, increasing the orientation angle was found to reduce both the specific compressive strength and modulus of elasticity of the lattice structure. An optimised lattice structure with strut diameter of 0.84 mm, length of 3.29 mm and orientation angle of 47° was shown to have specific compressive strength, elastic modulus, ultimate compression strength and porosity of 37.8 kN.m/kg, 1 GPa, 49.5 MPa and 85.7%, respectively. A cellular structure with the obtained properties could be effectively applied for trabecular bones replacement surgeries.

Keywords: *Additive Manufacturing; Implants; Porosity; Powder Bed Fusion; Lattices*

1. Introduction

Lattice structures are 3D open-celled porous structures which are topologically ordered and formed of repeatable units [1]. There are lattice structures available on nature such as wood, cork and bone (natural materials) as well as foam, honeycomb and sponges (synthetic technical materials). Typically, porous structures are classified to stochastic and non-stochastic. Lattice structures unit cells are composed of several struts connected at nodes. The unit cell is usually characterized by strut dimensions and connectivity. Despite that they are typically considered to have microstructures at the micro-scale level, they act as meta-materials when considering the overall structure [2-4].

Lattice structures can also be classified into strut-based and triply periodic minimal surfaces structures. Face-centred-cubic, body-centred-cubic, diamond, and octet-truss are the most used strut-based topologies. On the other hand, triply periodic minimal surface (TPMS) lattice structures include the Schoen gyroid, Neovius structures and Schwartz diamond. According to their mechanical behaviour, lattice structures are further classified into stretch-dominated and bending-dominated [5,6]. Bending-dominated behaviour is often experienced by stochastic or open-cell structures that encountered bending moments within their structure, causing them to be relatively ductile and deform more consistently. In contrast, stretch-dominated structures, which usually undergo axial loads, are more stiff and strong. Strut-based lattices, they are characterized by their Maxwell number "M", which could be determined as the following:

$$M = s - 3i - 6 \qquad \text{Eq1}$$

where "s" and "i" are the numbers of struts and nodes, respectively.

"M" always has a negative value for bending-dominated structures, indicating that the number of struts is not sufficient to withstand the applied stresses without balancing moments brought on at the nodes, which results in the generation of bending stresses in the lattice. However, when ($M \geq 0$), the applied load is transformed to axial tension and compression, eliminating the possibility of the occurrence of bending at nodes which results in stretch-dominated cellular structures. The low relative density is the most significant property of lattice structures (the fraction of solid structure). In addition, the high surface area of such

structures allows their use in applications such as filters, catalytic convertors, armours, heat exchangers, load-bearing components, and biomedical implants.

Several conventional manufacturing techniques have been used to fabricate lattice structures such as punching, powder metallurgy, investment casting, and metal foaming techniques [7]. However, the developed lattice structures produced consist often of a stochastic arrangement of either open or closed porosity (rather than an ordered porous structure) with a large variance of the shape and dimensions of the porosity [8]. In addition, microfabrication techniques, for example, lithography have also been used to fabricate sub-micrometer porous cellular structures [9], though lithography has been initially used for micro-electro-mechanical system devices [10-17]. These results in anisotropic mechanical properties, making the design of such structure more complicated. Nevertheless, these issues can be mitigated by using the emerged additive manufacturing (AM) technology which holds great potential in producing complex shapes and geometries that are unachievable by conventional manufacturing methods [18-22].

Additive manufacturing (AM), an important industry 4.0 technology, is an advanced manufacturing approach that has been developed and successfully applied applications such as biomedical [22], energy [23], aerospace [24,25], and defence [26,27]. Powder bed fusion (PBF) is one of the additive manufacturing techniques developed in the late 1980s, in which a 3D metal alloys or composites components are built layer-by-layer [28-30]. Powder bed fusion process begins with a digital CAD model representing the physical model, which is sliced into layers by special software. To build the physical object, a thin layer of the powder is spread over a substrate using a moving blade or a roller. Then, the desired 2D slice of the part geometry is obtained by selectively consolidating the powder using a laser beam. Next, another layer of the powder is spread, and the building process is repeated layer after layer until the full part is complete [31]. Different materials have been processed using PBF such as nickel, titanium and steels alloys, among them was the Ti6Al4V alloy. Owing to its exceptional biocompatibility and outstanding mechanical properties, Ti6Al4V is utilized broadly for the fabrication of medical implants and dental gadgets.

Since the beginning of the 21st century, the use of titanium alloys for biomedical applications have been receiving a great interest by industry and research. However, there are issues in using titanium alloys for bone implants. For example, the modulus of elasticity of Ti6Al4V is about 110 GPa, which is considerably larger than that of bone (10-30 GPa for cortical bones

and 0.02-1 GPa for trabecular or cancellous bones). Such stiffness mismatch was found to cause stress shielding and eventually result in the failure of the biomedical implant. To avoid the stress shielding between the implant and the bone, previous studies had recommended the use of porous titanium alloys, which have smaller stiffness and lighter when comparing to solid materials. In addition, the porosity of the implants allows body fluids and nutrition to move freely, which helps to improve the healing process. The use of lattice structures is one approach to achieve the required porosity of biomedical implants, which can go up to 98%. This might mimic the trabecular bones with porosity ranges from 50 to 90%. SLM is now classified as one of the most successful techniques that allow for the creation of porous lattices for different applications. [32-35].

PBF is a popular AM technique and has been widely used to metallic lattice structures. Compared to other additive manufacturing technologies, PBF was shown to provide better geometric accuracy and high resolution. In addition, the manufacturing of lattice structures, with their large surface areas and complex geometries using PBF is beneficial for heat dissipation during laser processing. As a result, the use of PBF for the fabrication of lattice structures was the focus of recent research. The focus in literature was to study the manufacturability of such structures and to analyse their mechanical behaviour [36]. One of the early studies was carried out by Brenne et al. [37] who experimentally investigated the compressive performance of AM-fabricated titanium BCC lattice structures. The authors reported the occurrence of shear failures along diagonal specimen planes. Many other researchers had also reported the significant effects of powder bed fusion parameters such as laser speed, power, and layer thickness on the mechanical properties of the developed lattice structures [38-40].

Design of experiment (DoE) is an inexpensive statistical modelling approach that is used for the analysis of the influence of different factors on specific responses of a component or a process. The use of design of experiments procedures such as analysis of variance (ANOVA), and the response surface method (RSM) has demonstrated to be effective in dealing with the impact of many factors and their interactions affecting the measured properties in material processing aiming to optimise the process [41]. RSM approach works by fitting the model curves by using the least-square method. The model accuracy is determined by using the ANOVA method [42]. Finally, the response surface graphs are used to construct the model surfaces and predict the optimum conditions. One of the widely used RSM tools is the central

composite design, in which each of the factors under investigation is set into +1, 0 and −1, levels. Two additional points are added for each factor at a distance of -α and +α from the basal (centre) point. A three-factor CCD design is shown in Figure 1. For many AM processes, RSM was effectively applied to evaluate the effect of process parameters on the quality of the components produced [33].

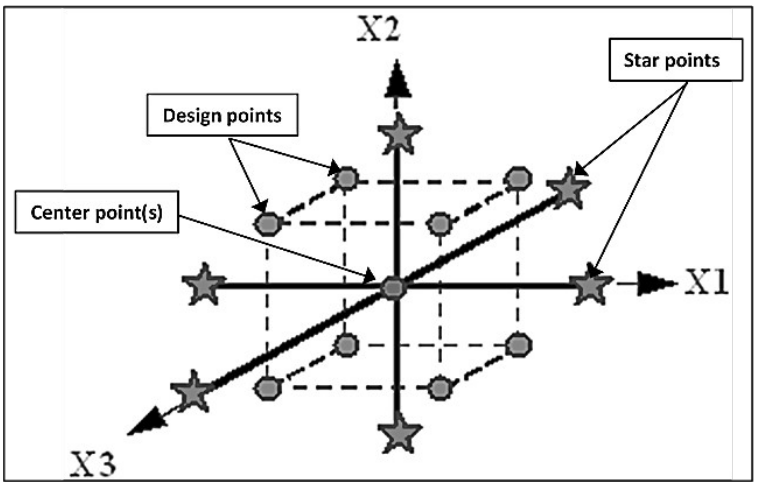

Figure 1: a central composite design for three factors.

Despite the reviewed research, the effect of lattice dimensions on the mechanical properties of the AM lattice structures is still lacking. Accordingly, this paper presents an attempt to understand the relationship between design parameters of the lattice unit cell such as strut diameter, length, and orientation angle on the compressive properties of Ti6Al4V lattice structures with diamond nodal unit cell produced by PBF process. DoE using ANOVA and of RSM will be adopted to optimize the unit cell design parameters to fabricate lattice structures with controlled compressive properties and Elastic modulus suitable for orthopaedic implants.

2. Experimental work

2.1 Materials

In this study Ti6Al4V gas-atomised powder, with a particle size of d_{50}=40 µm, supplied by TLS Technik GmbH was used. A scanning electron microscope image of the powder and the distribution of powder particle size are shown in Figure 2a,b. As shown, the powder particles are almost of spherical shape with different sizes and distributed homogeneously. The

Hausner' ratio of the powder was determined to be 1.16, indicating a reasonable flowability (good flowability < 1.25).

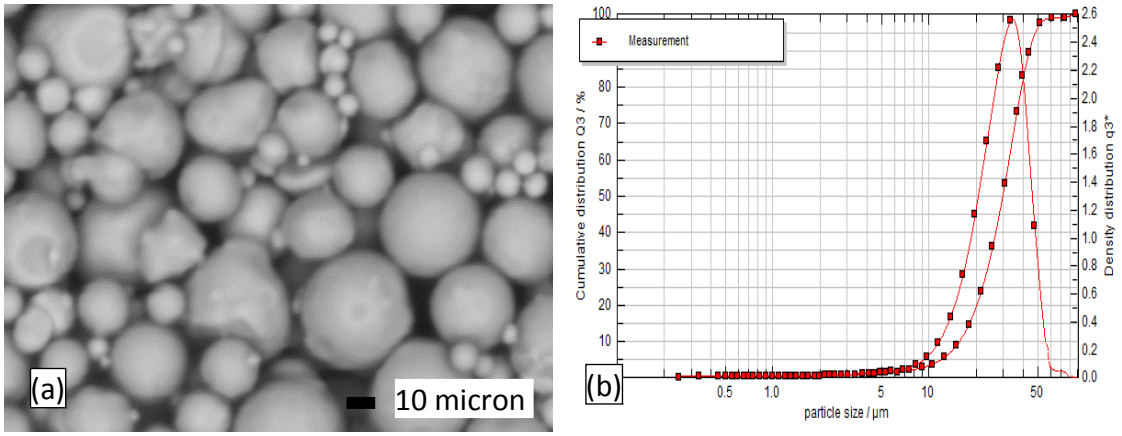

Figure 2: An SEM image of the powder particles, (b) powder particle size distribution

2.2 Experimental Design

Diamond unit cell is considered as a favourable lattice structure and hence has been used in orthopaedic applications [43,44]. A diamond lattice has an isotropic geometry that consists of four struts, which are connected nodally with another four struts. PBF has been extensively used to fabricate this type of structures at a large scale without distortion because of its self-supporting properties. A diamond unit cell lattice is illustrated in Figure 3. The most critical design parameters of this structure used in this study are the strut diameter (D), strut length (L) and the strut orientation angle (θ) [45,46].

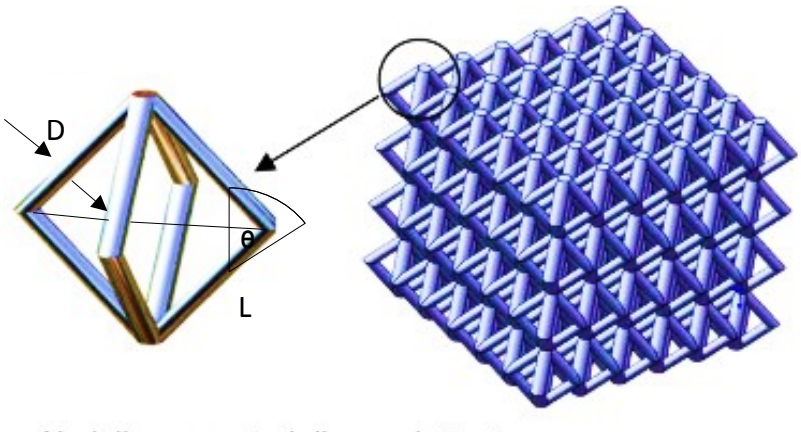

Figure 3: The diamond lattice structure with its design parameters

In this study, response surface approach using central composite design was employed to design the experimental plan and to study the effect of strut diameter (D), strut length (L) and the strut orientation angle on the compression properties of the PBF lattice structures. The dependent variable or the response "Y" is shown below as a 2nd order polynomial equation:

$$Y = \beta_o + \sum \beta_i x_i + \sum \beta_{ii} x_i^2 + \sum \beta_{ij} x_i x_j + \varepsilon (2)$$

where x_i, x_j are the independent variables (lattice design parameters) and ε is the residual term. The regression coefficients are expressed by β_0, β_i, β_{ii}, and β_{ij}, respectively. The processing of this statistical modelling was performed using Design-Expert Software which utilized the least-squares technique for the fitting of experimental data and subsequently, the calculation of regression (model) coefficients.

In the current central composite design, the three design parameters (independent variables) were varied over five levels (-α, -1, 0, 1, α), see Figure 1. The value of α is usually set to allow the design to be rotatable. Rotatable designs improve the quality of prediction of the model by ensuring a constant prediction variance at all points that are in halfway from the centre point. For a design with 3 factors, α should be equal to 1.682 to maintain rotatability of the design. The values of the different levels of the three factors are shown in Table 1, with their corresponding levels. Also, three centre points (at 0.6 mm strut diameter, 2.25 mm strut length and 45° orientation angle) were added to the design to allow the determination of the experimental error.

Table 1: Design matrix of the lattice structure design parameters and their levels

Variable	Symbol	Coded variable levels				
		Low (-1)	Central (0)	High (1)	- α	α
Strut Diameter (mm)	D	0.36	0.60	0.83	0.20	1.00
Strut Length (mm)	L	1.21	2.25	3.39	0.50	4.00
Strut Orientation Angle (°)	θ	36	45	54	30	60

2.3 Manufacturing and characterization

In this study, the diamond lattice structures were built up using Concept Laser M2 Cusing SLM system using the following parameters; layer thickness 0.02 mm, laser power 200 W and scan speed 1.2 m/s. To minimize the deviation during manufacture, the 17 samples were fabricated in a single batch. Afterwards, a wire electrical discharge machining (EDM) was employed to cut the cellular structures from the building plate. Examples of the printed lattice structures are shown in Figure 4.

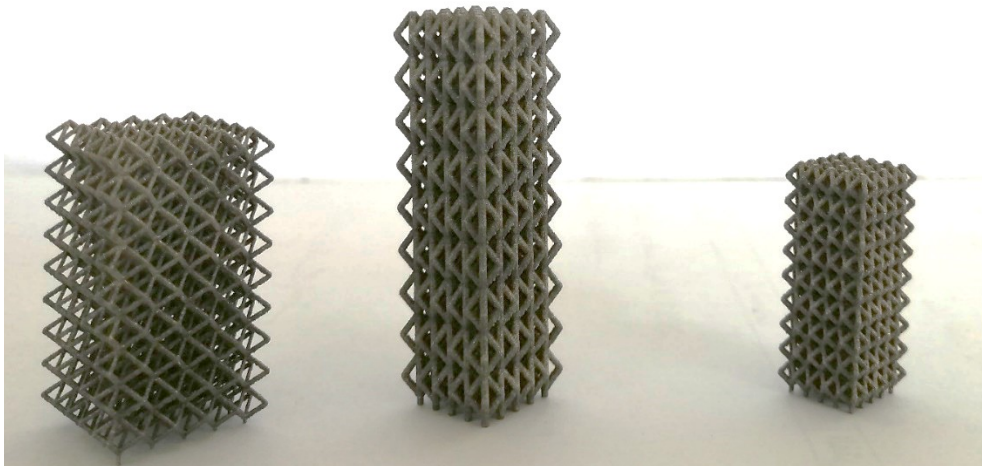

Figure 4: Ti6Al4V AM diamond lattice structures with different unit cell dimensions.

Samples were placed in Ultrasonic vibration in an acetone bath for 300 seconds to remove the trapped powder within the fabricated samples. Afterwards, a Mettler-Toledo densitometer device was used to measure the lattice density using based on the Archimedes principle. The measured density was divided by the parent alloy density (4420 kg/m^3) to determine the porosity of the cellular structure [47]. The compression properties of the prepared lattices were carried out using Zwick/Roell universal testing machine with a speed of 0.1 mm/min. All the samples were placed in the centre of the loading plate to ensure an even distribution of the compressive force during the test. The ultimate compressive strength (UCS) and modulus of elasticity of the as-fabricated samples were then determined. Finally, the specific compressive strength was calculated by dividing the UCS of the specimen by its density.

3. Results and discussion

Table 2 lists the 17 runs or parametric combinations along with the measured properties at each run. During compression testing, stress slowly increases without visible fracture of lattice struts to the ultimate strength of the structure. A rapid fall of the stress takes place after partial failures of lattice nodes due to the development of shear stresses. The compression stress increases again with further increasing of the strain until other nodes broke. The failure and picking up of stresses is repeated until the sample is split into pieces.

Table 2: Design matrix with resulting specific compressive strength, modulus of elasticity, UCS and porosity

Run	Struts diameter (mm)	Struts length (mm)	Orientation angle (degree)	Specific compressive strength (N·m/kg)	Modulus of elasticity (GPa)	UCS (MPa)	Porosity %
1	0.84	3.29	54	24595	0.35	19.3	82.4
2	0.60	2.25	60	26678	0.44	26.1	78.1
3	0.36	1.21	36	121075	9.59	150.0	26.4
4	0.36	3.29	54	12122	0.05	3.7	93.2
5	0.60	2.25	30	119811	7.73	184.5	65.5
6	0.84	3.29	36	68639	1.55	82.4	73.1
7	0.60	2.25	45	44155	1.28	47.3	75.0
8	0.20	2.25	45	21651	0.22	10.2	89.4
9	0.36	1.21	54	58143	4.95	145.8	43.9
10	0.84	1.21	54	43269	4.19	68.7	64.5
11	0.60	4.00	45	17210	0.16	7.5	90.3
12	0.36	3.29	36	21512	0.26	8.8	90.8
13	0.60	0.50	45	110718	11.83	200.0	20.0
14	0.84	1.21	36	43958	9.31	95.5	51.4
15	1.00	2.25	45	114723	8.34	228.4	55.5
16	0.60	2.25	45	46801	1.41	52.2	74.8
17	0.60	2.25	45	43785	1.17	49.3	76.0

3.1 ANOVA results

Model fitting analysis indicated that the best-fitted model is approximately linear for the four measured properties. Figures 5 (a), (b), (c) and (d) show the normal probability graphs of the residuals of the specific compressive strength, modulus of elasticity, UCS and porosity% respectively. In addition, the plots of the residuals-versus-run of the four responses are shown in Figure 6 (a), (b) (c) and (d), respectively. The plotted data in Figure 6 indicated the lack of

unusual structure. Such observations suggested that the proposed models do not violate the assumption of normality and independence of residuals and hence it had been adopted for the subsequent analysis

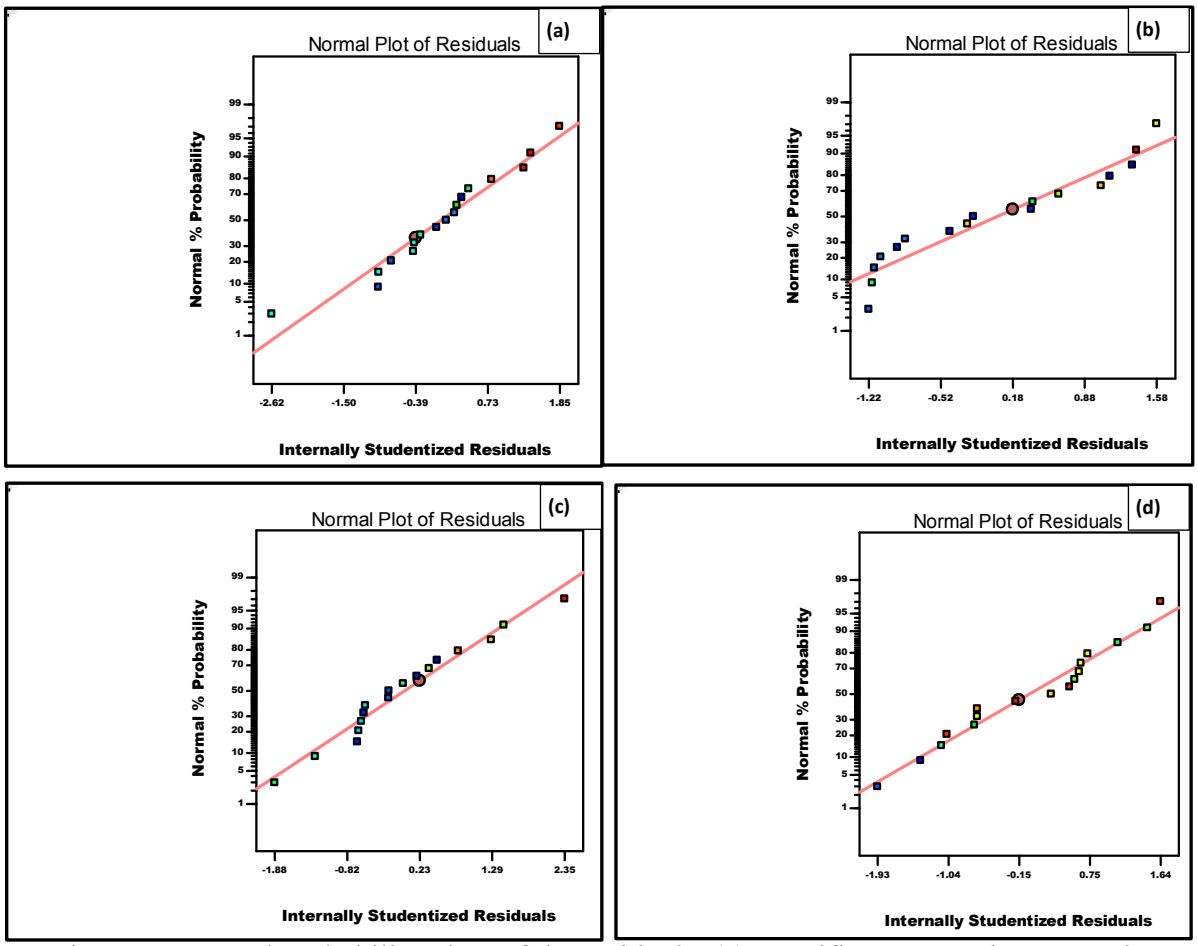

Figure 5: Normal probability plots of the residuals. (a) Specific compressive strength, (b) modulus of elasticity, (c) UCS, and (d) porosity %.

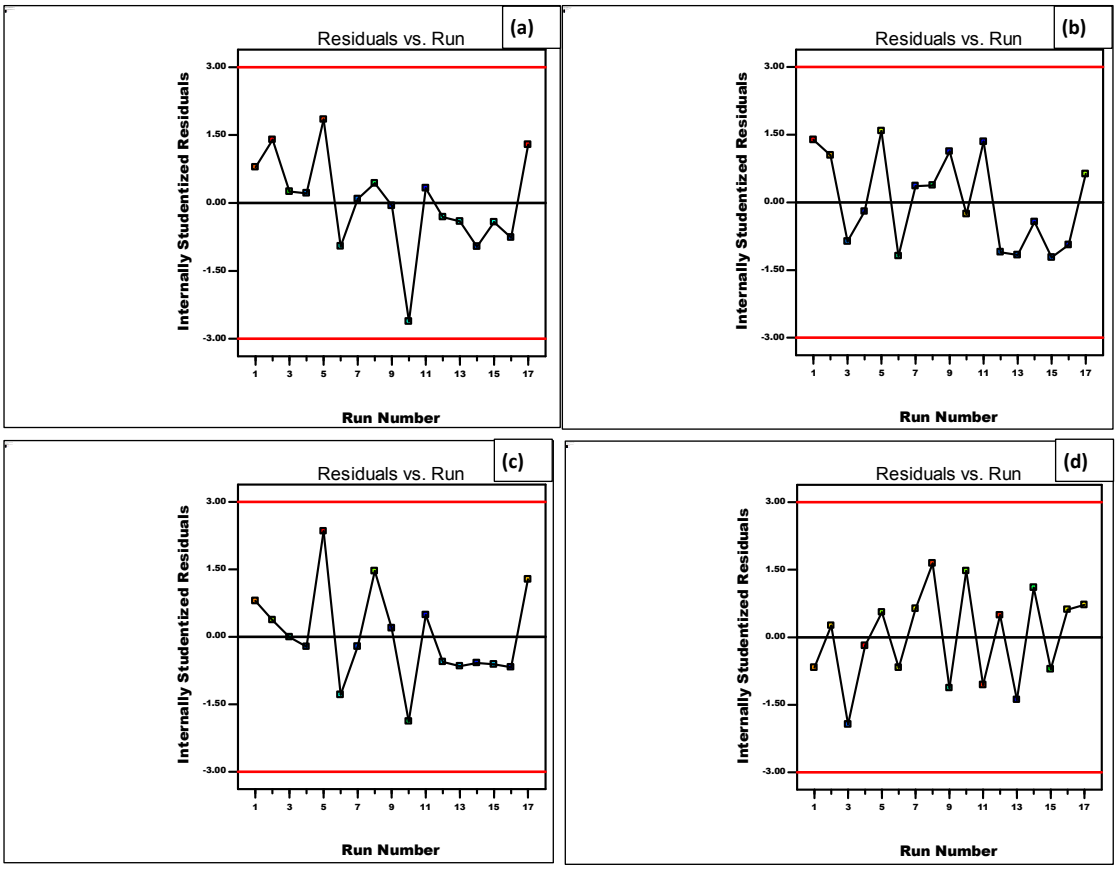

Figure 6: Plots of residuals vs run. (a) specific compressive strength, (b) modulus of elasticity, (c) UCS, and (d) porosity %.

The general empirical linear equation that represents the responses of interest in terms of strut Diameter (D), Length (L) and Orientation angle (O) is given as the following:

$$Response = \beta_o + \beta_1(D) + \beta_2(L) + \beta_3(O) \qquad (3)$$

Where β_o, β_1, β_2 and β_3 are the regression coefficients (see above) that depend on the main effects of the lattice design parameters. The data analysis performed by Design Expert based on least-squares fitting resulted in the determination of required coefficients of the model equations representing the responses of interest in this study. Table 3 lists the values of the coefficients.

Table 3: Regression constants for the specific compressive strength, elastic modulus, UCS and porosity %

Model Constant	Specific compressive strength	Modulus of elasticity	UCS	Porosity %
βo	+1.80405E+005	+16.93192	+262.36533	+8.60553
β1	+38217.59776	+4.37441	+99.89759	-12.33752
β2	-20888.33964	-3.19995	-47.12801	+19.12782
β3	-2246.90201	-0.19248	-3.00239	+0.52089

ANOVA has determined the significance of each of the design parameters and for each response through the calculation of the *p*-value. A *p*-value <0.05 indicated a significant influence of the design parameter on the measured property of the lattice structure [33]. The p-values of each of the model parameters for the four responses are listed in Table 4. It was suggested that the strut length and strut orientation angle were found to significantly affect both the specific compressive strength and modulus of elasticity. In addition, the UCS and porosity % were both mainly influenced by the strut length. It was suggested that the effect of both the strut diameter on the modulus of elasticity and the effect of the orientation angle on the UCS were of less significance.

Table 4: p-values of the model terms for the specific compressive strength, modulus of elasticity, UCS and porosity %.

Model Parameter	p-value			
	Specific compressive strength	Modulus of elasticity	UCS	Porosity %
D	0.2511	0.0950	0.1236	0.3808
L	**0.0131**	**< 0.0001**	**0.0048**	**< 0.0001**
O	**0.0201**	**0.0108**	0.0863	0.1746

*Bold values indicate statistically significant model term (p-value<0.05). Values higher than 0.1000 indicate the parameter is not significant.

3.2 Analysis of specific compressive strength

The specific compressive strength was shown to be significantly affected by both the strut length and orientation angle. Figure 7 shows that increasing the strut length from 1.21 to 3.29

mm, while keeping the strut diameter and orientation angle at 0.6 mm and 45°, respectively. As shown, there is a considerable reduction in the specific compressive strength from 77 to 33.5 kN·m/kg. Similarly, the specific compressive strength was found to decrease from 75.3 to 35.2 kN·m/kg as a result of increasing the orientation angle from 36 to 54°, at constant strut diameter and strut length of 0.6 mm and 2.25 mm respectively.

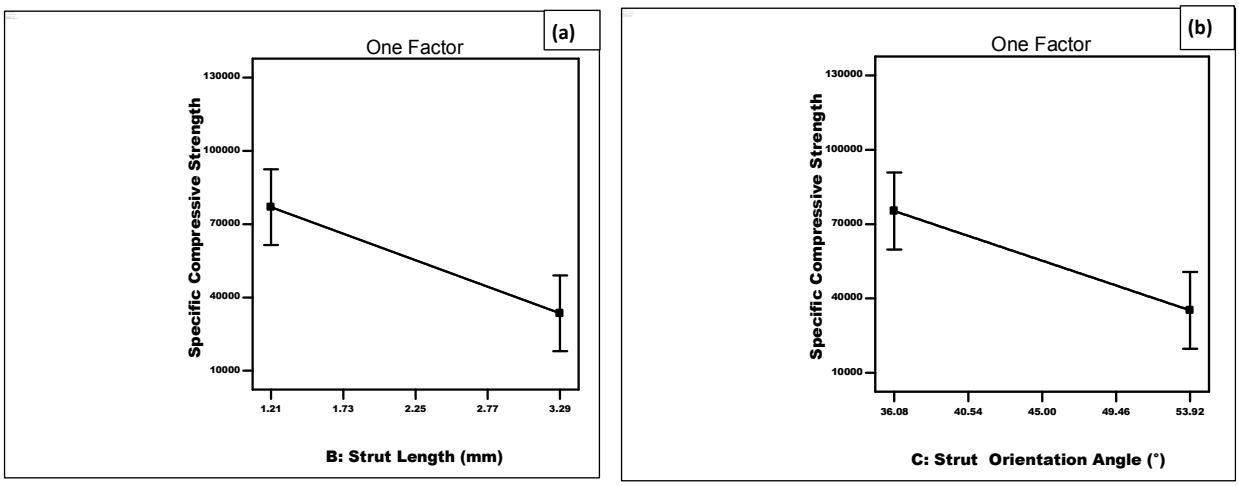

Figure 7: Effect of (a) strut length and (b) orientation angle on the specific compressive strength.

3.3 Analysis of modulus of elasticity

Figures 8 (a), (b) and (c) show the linear model graphs of the effect of strut diameter, length, and orientation angle, respectively, on the elastic modulus. As shown, the elastic modulus increases with larger strut diameters and/or smaller strut lengths and orientation angles. Increasing the strut diameters and decreasing the strut lengths reduces the structure porosity, which increases the stiffness of the samples whereas increasing the orientation angle reduces the developed shear stresses, which also improve the stiffness of the sample against the applied load.

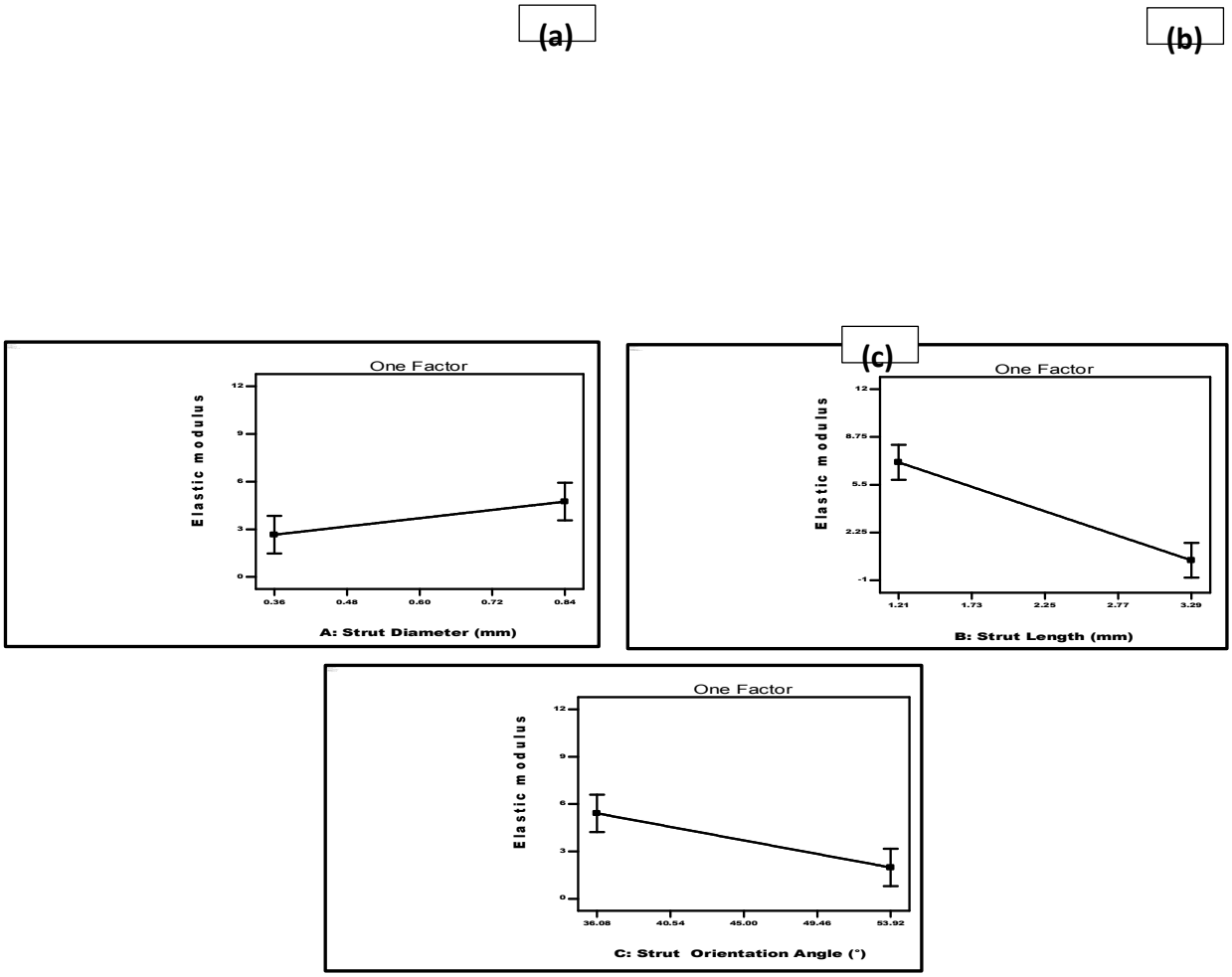

Figure 8. Main effect of (a) strut diameter, (b) length and (c) orientation angle on the modulus of elasticity.

3.4 Analysis of UCS

The main effect of strut length and strut orientation angle on the UCS is shown in Figures 9 (a) and (b) respectively. Both design parameters were suggested to inversely affecting the UCS.

(a) (b)

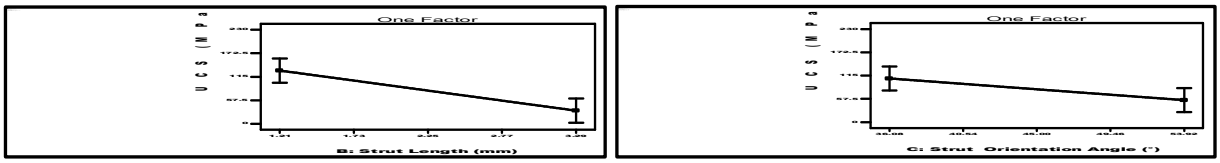

Figure 9. Effect of (a) strut length and (b) orientation angle on the UCS.

3.5 Porosity analysis

Again, and referring to Table 4, only the strut length was found affecting the porosity %, as shown in Figure 10. At constant strut diameter of 0.6 mm and constant orientation angle of 45°, increasing the strut length from 1.21 to 3.29 mm caused the porosity % to be remarkably increased from 48 to 88%.

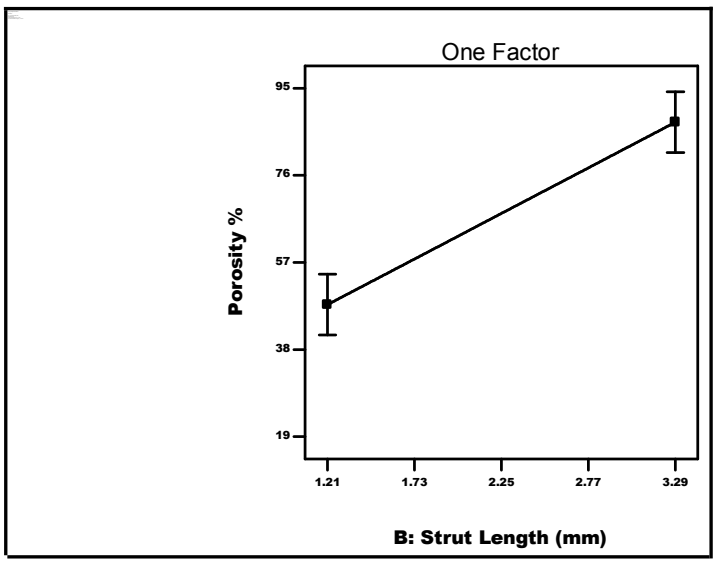

Figure 10. Effect of strut length on porosity %.

3.6 Optimization of lattice properties towards bone replacement

Given its high strength and stiffness to weight ratios, Ti6Al4V is a preferred candidate for biomedical implants and scaffolds using PBF. As described above, the properties of the implant should, to a great extent, mimic those of the host bone and surrounding tissues. For this reason, a fully solid Ti6Al4V is unsuitable due to its impermeability which prohibiting the transporting of body fluids and medication. In addition, the elastic modulus of Ti6Al4V (≈110 GPa) is much higher that of human bones (about two to three orders higher comparing to trabecular and cancellous bones). This results in the stress shielding of the bone tissue and ultimately could result in the failure of the implant surgery. These problems can be addressed by the design optimization of the biomedical implant which should integrate both the adequate mechanical strength and porosity to allow the orthopaedic implant to have both sufficient strength and Elastic modulus to withstand the applied stresses and appropriate porosity to assist the flow of body nutrients. Lui et al. [47] concluded that out controlling Young's modulus of Ti6Al4V AM-fabricated structures for trabecular bones is essential to overcome the stress shielding problem. In order to optimise the design parameters of the lattice geometry for trabecular bones replacement, surface response predictor was applied to perform a multi-response optimization. The gaols were to maximize both the specific compressive strength and UCS while attaining Young's modulus from 0.02 and 1 GPa, and porosity % that ranges between 50 and 90 (typical ranges for trabecular bones) [35]. Considering the measured values of the responses and the model coefficients (described in Tables 2 and 3 respectively), the response equations describing the specific compressive strength, modulus of elasticity, UCS and porosity % were solved simultaneously to prophesy the lattice cell design parameters that fulfil desired optimization goals.

Figures 11 (a), (b), (c) and (d) show the optimization contour of specific compressive strength, modulus of elasticity, UCS and porosity % respectively, for a range of strut diameter (0.2-1 mm) and strut length (0.5-4 mm). The predicted optimized values of the diamond cell dimensions would be 0.84 mm strut diameter, 3.29 mm length and 47° orientation angle. The corresponding measured properties of the optimised structure were 37.8 kN.m/kg, 1 GPa, 49.5 MPa and 85.7% for the specific strength, Elastic modulus, compression strength, and porosity.

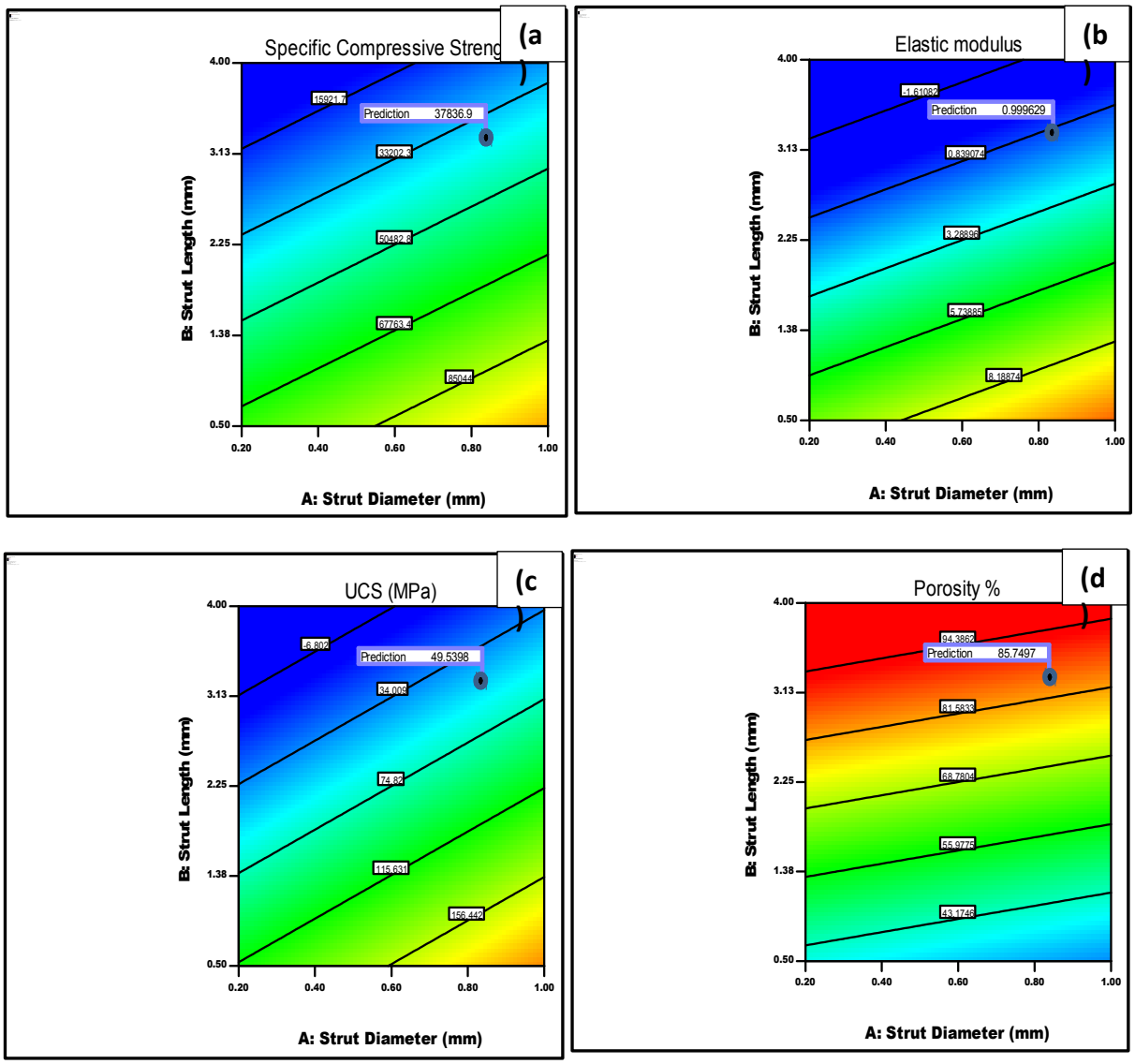

Figure 11. Predicted optimum strut diameter and strut length (at a strut orientation angle of 47°) of a Ti6Al4V diamond lattice structure for medical implants; (a) maximum specific compressive strength, (b) elastic modulus (0.02-1 GPa), (c) highest UCS, and (d) porosity % (50-90).

Previous studies used PBF to control the solid volume fraction of cellular structures customized for orthopaedic applications. These studies showed the possibility of manufacturing scaffolds with porosity levels and adequate properties for osteointegration. In a study by Weißmann et al. [48], Ti6Al4V truncated pyramid lattice structures were fabricated using PBF with 80% porosity. The predicted equivalent modulus of elasticity and UCS were 3.4 GPa and 121 MPa, respectively. Nevertheless, the diamond lattice with optimized properties in the present study have a porosity level of 85.7%, and the corresponding modules

of elasticity and UCS were 1 GPa and 49.5 MPa, respectively [48]. This discrepancy is apparently reasoned to the different lattice types used in both studies. In the present study, a diamond lattice structure was fabricated while in the research by Weißmann pyramidal design was employed. Another study by Liu et al., diamond unit cell lattices were produced from Ti6Al4V with different densities in order to mimic those of human bones. The authors reported the success of fabricating a lattice structure with porosity %, modulus of elasticity and UCS of about 86.7%, 0.82 GPa and 42.5 MPa respectively, which are not far from the properties obtained using the optimized lattice structure in the present work [47]. In another study of Ti6Al4V lattices manufactured via PBF, Choy and co-authors compared the deformation behaviour of cubic and honeycomb lattice structures for different orientations and densities. Their results suggested that the struts orientation angle significantly affected the developed stresses [49].

The recommended values for lattice unit cell design parameters that could be used for bone replacement surgeries were investigated. Three identical lattice structures were fabricated by PBF with the optimized lattice dimensions. The porosity % and compressive properties of the three lattices were examined, and the average measured values were 37.8 kN.m/kg, 0.97 GPa, 44.3 MPa and 87.3% for the specific compressive strength, elastic modulus, UCS and porosity% respectively. The error in model prediction was less than 10%, suggesting the robustness of the model in estimating the optimum lattice unit cell dimensions orthopaedic bone implants.

4. Conclusions

In this study, the influence of lattice design parameters of Ti6Al4V diamond lattices, manufactured using PBF, on the compressive properties and porosity of the cellular structure was investigated by means of response surface and ANOVA statistical analysis techniques. In addition, the lattice dimensions were optimized to fabricate a diamond cellular structure with properties that match human bones. The key findings of this study are listed below:

1. The most significant design parameter of the unit cell was the strut length. It was suggested by the ANOVA to remarkably affect the porosity % in a direct relationship, while it had a significant reverse effect on the specific compressive strength, elastic modulus and UCS.

2. Increasing the orientation angle was found to significantly reduce both the specific compressive strength and modulus of elasticity of the lattice structure.
3. An optimised diamond lattice with strut diameter, length and orientation angle of 0.84 mm, 3.29 mm and 47° respectively was shown to have specific compressive strength, elastic modulus, UCS and porosity % of 37.8 kN.m/kg, 1 GPa, 49.5 MPa and 85.7, respectively. A cellular structure with such properties could be effectively applied for trabecular bones replacement surgeries.

References

1. Kang, D.; Park, S.; Son, Y.; Yeon, S.; Kim, S.H.; Kim, I. Multi-lattice inner structures for high-strength and light-weight in metal selective laser melting process. *Materials & Design* **2019**, *175*, 107786.
2. Iwase, A.; Hori, F. Modification of Lattice Structures and Mechanical Properties of Metallic Materials by Energetic Ion Irradiation and Subsequent Thermal Treatments. *Quantum Beam Science* **2020**, *4*, 17.
3. Cosma, C.; Kessler, J.; Gebhardt, A.; Campbell, I.; Balc, N. Improving the Mechanical Strength of Dental Applications and Lattice Structures SLM Processed. *Materials* **2020**, *13*, 905.
4. Sienkiewicz, J.; Płatek, P.; Jiang, F.; Sun, X.; Rusinek, A. Investigations on the Mechanical Response of Gradient Lattice Structures Manufactured via SLM. *Metals* **2020**, *10*, 213.
5. Maconachie, T.; Leary, M.; Lozanovski, B.; Zhang, X.; Qian, M.; Faruque, O.; Brandt, M. SLM lattice structures: Properties, performance, applications and challenges. *Materials & Design* **2019**, 108137.
6. Maskery, I.; Aremu, A.; Parry, L.; Wildman, R.; Tuck, C.; Ashcroft, I. Effective design and simulation of surface-based lattice structures featuring volume fraction and cell type grading. *Materials & Design* **2018**, *155*, 220-232.
7. Narkhede, S.; Sur, A.; Darvekar, S. Applications, manufacturing and thermal characteristics of micro-lattice structures: Current state of the art. *Engineering Journal* **2019**, *23*, 419-431, doi:10.4186/ej.2019.23.6.419.
8. Rashed, M.; Ashraf, M.; Mines, R.; Hazell, P.J. Metallic microlattice materials: A current state of the art on manufacturing, mechanical properties and applications. *Materials & Design* **2016**, *95*, 518-533.
9. Maldovan, M.; Ullal, C.K.; Jang, J.-H.; Thomas, E.L. Sub-Micrometer Scale Periodic Porous Cellular Structures: Microframes Prepared by Holographic Interference Lithography. *Advanced Materials* **2007**, *19*, 3809-3813, doi:10.1002/adma.200700811.
10. Zhu, Z.; Hassanin, H.; Jiang, K. A soft moulding process for manufacture of net-shape ceramic microcomponents. *The International Journal of Advanced Manufacturing Technology* **2010**, *47*, 147-152, doi:10.1007/s00170-008-1864-z.
11. Hassanin, H.; Jiang, K. Multiple replication of thick PDMS micropatterns using surfactants as release agents. *Microelectronic Engineering* **2011**, *88*, 3275-3277, doi:https://doi.org/10.1016/j.mee.2011.06.027.

12. Hassanin, H.; Jiang, K. Fabrication of Al2O3/SiC Composite Microcomponents using Non-aqueous Suspension. *Advanced Engineering Materials* **2009**, *11*, 101-105, doi:10.1002/adem.200800158.
13. Hassanin, H.; Jiang, K. Net shape manufacturing of ceramic micro parts with tailored graded layers. *Journal of Micromechanics and Microengineering* **2013**, *24*, 015018, doi:10.1088/0960-1317/24/1/015018.
14. Hassanin, H.; Jiang, K. Fabrication and characterization of stabilised zirconia micro parts via slip casting and soft moulding. *Scripta Materialia* **2013**, *69*, 433-436, doi:https://doi.org/10.1016/j.scriptamat.2013.05.004.
15. Hassanin, H.; Jiang, K. Functionally graded microceramic components. *Microelectronic Engineering* **2010**, *87*, 1610-1613, doi:https://doi.org/10.1016/j.mee.2009.10.044.
16. Hassanin, H.; Jiang, K. Alumina composite suspension preparation for softlithography microfabrication. *Microelectronic Engineering* **2009**, *86*, 929-932, doi:https://doi.org/10.1016/j.mee.2008.12.067.
17. Hassanin, H.; Jiang, K. Optimized process for the fabrication of zirconia micro parts. *Microelectronic Engineering* **2010**, *87*, 1617-1619, doi:https://doi.org/10.1016/j.mee.2009.10.037.
18. Essa, K.; Modica, F.; Imbaby, M.; El-Sayed, M.A.; ElShaer, A.; Jiang, K.; Hassanin, H. Manufacturing of metallic micro-components using hybrid soft lithography and micro-electrical discharge machining. *The International Journal of Advanced Manufacturing Technology* **2017**, *91*, 445-452.
19. Hassanin, H.; Essa, K.; Qiu, C.; Abdelhafeez Ali, M.; Adkins Nicholas, J.E.; Attallah Moataz, M. Net-shape manufacturing using hybrid selective laser melting/hot isostatic pressing. *Rapid Prototyping Journal* **2017**, *23*, 720-726, doi:10.1108/RPJ-02-2016-0019.
20. Qiu, C.; Adkins, N.J.E.; Hassanin, H.; Attallah, M.M.; Essa, K. In-situ shelling via selective laser melting: Modelling and microstructural characterisation. *Materials & Design* **2015**, *87*, 845-853, doi:https://doi.org/10.1016/j.matdes.2015.08.091.
21. Hassanin, H.; Finet, L.; Cox, S.C.; Jamshidi, P.; Grover, L.M.; Shepherd, D.E.T.; Addison, O.; Attallah, M.M. Tailoring selective laser melting process for titanium drug-delivering implants with releasing micro-channels. *Additive Manufacturing* **2018**, *20*, 144-155, doi:https://doi.org/10.1016/j.addma.2018.01.005.
22. Klippstein, H.; Hassanin, H.; Diaz De Cerio Sanchez, A.; Zweiri, Y.; Seneviratne, L. Additive Manufacturing of Porous Structures for Unmanned Aerial Vehicles Applications. *Advanced Engineering Materials* **2018**, *20*, 1800290, doi:10.1002/adem.201800290.
23. Sabouri, A.; Yetisen, A.K.; Sadigzade, R.; Hassanin, H.; Essa, K.; Butt, H. Three-Dimensional Microstructured Lattices for Oil Sensing. *Energy & Fuels* **2017**, *31*, 2524-2529, doi:10.1021/acs.energyfuels.6b02850.
24. Klippstein, H.; Diaz De Cerio Sanchez, A.; Hassanin, H.; Zweiri, Y.; Seneviratne, L. Fused Deposition Modeling for Unmanned Aerial Vehicles (UAVs): A Review. *Advanced Engineering Materials* **2018**, *20*, 1700552, doi:10.1002/adem.201700552.
25. Galatas, A.; Hassanin, H.; Zweiri, Y.; Seneviratne, L. Additive Manufactured Sandwich Composite/ABS Parts for Unmanned Aerial Vehicle Applications. *Polymers (Basel)* **2018**, *10*, 1262.
26. Tan, C.; Li, S.; Essa, K.; Jamshidi, P.; Zhou, K.; Ma, W.; Attallah, M.M. Laser Powder Bed Fusion of Ti-rich TiNi lattice structures: Process optimisation, geometrical integrity, and phase transformations. *International Journal of Machine*

Tools and Manufacture **2019**, *141*, 19-29, doi:https://doi.org/10.1016/j.ijmachtools.2019.04.002.
27. Hassanin, H.; Abena, A.; Elsayed, M.A.; Essa, K. 4D Printing of NiTi Auxetic Structure with Improved Ballistic Performance. *Micromachines* **2020**, *11*, 745.
28. Penchev, P.; Bhaduri, D.; Carter, L.; Mehmeti, A.; Essa, K.; Dimov, S.; Adkins, N.J.E.; Maillol, N.; Bajolet, J.; Maurath, J., et al. System-level integration tools for laser-based powder bed fusion enabled process chains. *Journal of Manufacturing Systems* **2019**, *50*, 87-102, doi:https://doi.org/10.1016/j.jmsy.2018.12.003.
29. Li, Y.; Feng, Z.; Hao, L.; Huang, L.; Xin, C.; Wang, Y.; Bilotti, E.; Essa, K.; Zhang, H.; Li, Z., et al. A Review on Functionally Graded Materials and Structures via Additive Manufacturing: From Multi-Scale Design to Versatile Functional Properties. *Advanced Materials Technologies* **2020**, *5*, 1900981, doi:10.1002/admt.201900981.
30. Li, Y.; Feng, Z.; Huang, L.; Essa, K.; Bilotti, E.; Zhang, H.; Peijs, T.; Hao, L. Additive manufacturing high performance graphene-based composites: A review. *Composites Part A: Applied Science and Manufacturing* **2019**, *124*, 105483, doi:https://doi.org/10.1016/j.compositesa.2019.105483.
31. Rehme, O.; Emmelmann, C. *Rapid manufacturing of lattice structures with selective laser melting*; SPIE: 2006; Vol. 6107.
32. Challis, V.J.; Xu, X.; Zhang, L.C.; Roberts, A.P.; Grotowski, J.F.; Sercombe, T.B. High specific strength and stiffness structures produced using selective laser melting. *Materials & Design* **2014**, *63*, 783-788.
33. Elsayed, M.; Ghazy, M.; Youssef, Y.; Essa, K. Optimization of SLM process parameters for Ti6Al4V medical implants. *Rapid Prototyping Journal* **2019**, *25*, 433-447.
34. Hassanin, H.; Al-Kinani, A.A.; ElShaer, A.; Polycarpou, E.; El-Sayed, M.A.; Essa, K. Stainless steel with tailored porosity using canister-free hot isostatic pressing for improved osseointegration implants. *Journal of Materials Chemistry B* **2017**, *5*, 9384-9394.
35. Wang, X.; Xu, S.; Zhou, S.; Xu, W.; Leary, M.; Choong, P.; Qian, M.; Brandt, M.; Xie, Y.M. Topological design and additive manufacturing of porous metals for bone scaffolds and orthopaedic implants: A review. *Biomaterials* **2016**, *83*, 127-141.
36. Sing, S.L.; Yeong, W.Y.; Wiria, F.E.; Tay, B. Characterization of titanium lattice structures fabricated by selective laser melting using an adapted compressive test method. *Experimental Mechanics* **2016**, *56*, 735-748.
37. Brenne, F.; Niendorf, T.; Maier, H. Additively manufactured cellular structures: Impact of microstructure and local strains on the monotonic and cyclic behavior under uniaxial and bending load. *Journal of Materials Processing Technology* **2013**, *213*, 1558-1564.
38. Salem, H.; Carter, L.; Attallah, M.; Salem, H. Influence of processing parameters on internal porosity and types of defects formed in Ti6Al4V lattice structure fabricated by selective laser melting. *Materials Science and Engineering: A* **2019**, *767*, 138387.
39. Wauthle, R.; Vrancken, B.; Beynaerts, B.; Jorissen, K.; Schrooten, J.; Kruth, J.-P.; Van Humbeeck, J. Effects of build orientation and heat treatment on the microstructure and mechanical properties of selective laser melted Ti6Al4V lattice structures. *Additive Manufacturing* **2015**, *5*, 77-84.
40. Mazur, M.; Leary, M.; Sun, S.; Vcelka, M.; Shidid, D.; Brandt, M. Deformation and failure behaviour of Ti-6Al-4V lattice structures manufactured by selective laser melting (SLM). *The International Journal of Advanced Manufacturing Technology* **2016**, *84*, 1391-1411.

41. Sing, S.L.; Wiria, F.E.; Yeong, W.Y. Selective laser melting of lattice structures: A statistical approach to manufacturability and mechanical behavior. *Robotics and Computer-Integrated Manufacturing* **2018**, *49*, 170-180.
42. Hader, R.; Park, S.H. Slope-rotatable central composite designs. *Technometrics* **1978**, *20*, 413-417.
43. Tamburrino, F.; Graziosi, S.; Bordegoni, M. The design process of additively manufactured mesoscale lattice structures: A review. *Journal of Computing and Information Science in Engineering* **2018**, *18*, doi:10.1115/1.4040131.
44. Essa, K.; Hassanin, H.; Attallah, M.M.; Adkins, N.J.; Musker, A.J.; Roberts, G.T.; Tenev, N.; Smith, M. Development and testing of an additively manufactured monolithic catalyst bed for HTP thruster applications. *Applied Catalysis A: General* **2017**, *542*, 125-135, doi:https://doi.org/10.1016/j.apcata.2017.05.019.
45. Hassanin, H.; Alkendi, Y.; Elsayed, M.; Essa, K.; Zweiri, Y. Controlling the properties of additively manufactured cellular structures using machine learning approaches. *Advanced Engineering Materials* **2020**.
46. Essa, K.; Sabouri, A.; Butt, H.; Basuny, F.H.; Ghazy, M.; El-Sayed, M.A. Laser additive manufacturing of 3D meshes for optical applications. *PloS one* **2018**, *13*.
47. Liu, F.; Zhang, D.Z.; Zhang, P.; Zhao, M.; Jafar, S. Mechanical properties of optimized diamond lattice structure for bone scaffolds fabricated via selective laser melting. *Materials* **2018**, *11*, 374.
48. Weißmann, V.; Wieding, J.; Hansmann, H.; Laufer, N.; Wolf, A.; Bader, R. Specific yielding of selective laser-melted Ti6Al4V open-porous scaffolds as a function of unit cell design and dimensions. *Metals* **2016**, *6*, 166.
49. Choy, S.Y.; Sun, C.-N.; Leong, K.F.; Wei, J. Compressive properties of Ti-6Al-4V lattice structures fabricated by selective laser melting: Design, orientation and density. *Additive Manufacturing* **2017**, *16*, 213-224.